ICIC Express Letters
Part B: Applications
Volume **10**, Number **6**, June **2019**

ICIC International ©2019 ISSN 2185-2766
pp. **491–499**

MODELING AND GENERALIZED PREDICTIVE CONTROL STRATEGY OF A MICRO GAS TURBINE

Jianhua Zhang[1,2], Jijun Cao[2], Penghao Fan[2], Guanglei Cui[2]
Zhiqiang Wu[2] and Pansheng Wang[2]

[1]State Key Laboratory of Alternate Electrical Power System with Renewable Energy Sources
[2]School of Control and Computer Engineering
North China Electric Power University
No. 2, Beinong Road, Changping District, Beijing 102206, P. R. China
zjh@ncepu.edu.cn

Received November 2018; accepted February 2019

Abstract. *Micro Gas Turbine (MGT) is one of the key technologies in the field of energy and power system. In this paper, the physical model of a WR100 MGT is established by integrating sub-models of the compressor, combustor, and turbine. And then a Generalized Predictive Controller (GPC) is designed. In the simulation phase, both the set-point tracking ability test and anti-disturbance ability test are carried out. Compared with the traditional PID controller, the generalized predictive controller shows better control performance.*
Keywords: Micro Gas Turbine (MGT), Modeling, Generalized Predictive Controller (GPC), Simulation

1. **Introduction.** MGT power generation systems have been applied in practice. It can be acted as a power generation device for a distributed power supply system or a supplemental power generation device for a centralized power supply system. In order to ensure safe, reliable and economical operation of MGT power generator units, it is crucial to study the dynamic characteristics of MGT power generator units. It is usually difficult to carry out field tests directly on the MGT generator unit, because the field test has a very high demand for outdoor temperature [1]. Therefore, a suitable MGT generator unit dynamic performance simulation model was established in [2], and the built model of MGT power generator systems plays an important role in system design, performance analysis and on-site commissioning.

The dynamic characteristics of MGT power generation systems is complicated in terms of nonlinearities, coupling and uncertainties [3,7]. Hence, it is necessary to design control system for improving power generation efficiency. An automatic generation control strategy was presented using traditional controllers based on the Firefly algorithm [4]. Following predictive control algorithms in [5,6,8], a generalized predictive control algorithm based on Controlled Auto-Regressive Integrated Moving-Average (CARIMA) model is applied into MGT power generation systems in this paper.

The reminder of this paper is organized as follows. Section 2 builds a model for MGT power generation systems. Section 3 summarizes GPC algorithm. Section 4 applies GPC into an MGT power generation system, and some simulation results are then shown to illustrate the effectiveness and feasibility of the proposed approach. Finally, some conclusions are drawn in Section 5.

DOI: 10.24507/icicelb.10.06.491

2. **System Modeling.** The diagram of an MGT with reheater is shown in Figure 1. The main components include the turbine, the compressor and the combustion chamber. In practice, the turbine outlet temperature during the simple cycle is still relatively high. In order to deeply utilize the waste heat and improve the efficiency of the MGT system, a high-efficiency reheater is installed in this MGT power generation system. The regenerative cycle increases the preheating of the compressed air. The modeling process of each component is described as Figure 1.

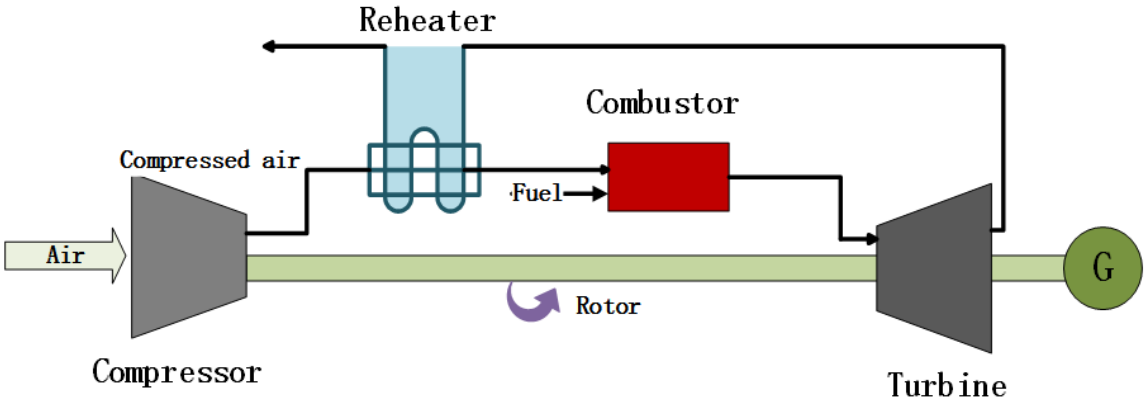

FIGURE 1. Diagram of MGT with reheater

2.1. **The flow continuity equation of the MGT.** Gas mass flow rate is mainly dependent on the air mass flow rate inhaled by the compressor, and it can be described by:

$$m_g = \mu_a m_a \tag{1}$$

where m_g and m_a are gas mass flow rate that has passed turbine in unit time and the air mass flow rate inhaled by the compressor respectively, and μ_a stands for the flow difference factor.

The characteristic curves of the compressor and the turbine can be plotted according to

$$m_a = f(n, p_2) = f(n, \pi_C) \tag{2}$$

and

$$m_g = f(T_4, p_4) \tag{3}$$

where n and π_C are the rotor speed and the compressor pressure ratio respectively, p_2 stands for the compressor outlet pressure, T_4 the turbine inlet temperature and p_4 the turbine inlet pressure.

According to the compressor characteristic curve and the turbine characteristic curve, Equation (1) can be reformulated as follows by a small deviation linearization method

$$\overline{p_2} = K_{1n}\overline{n} + K_{1T_4}\overline{T_4} \tag{4}$$

where K_{1T_4}, the coefficient of action of $\overline{p_2}$ for $\overline{T_4}$, and K_{1n}, the coefficient of action of $\overline{p_2}$ for $\overline{n}$, can be calculated by

$$K_{1T_4} = -T_{40}(\partial m_g/\partial T_4)/[p_{40}(\partial m_g/\partial p_4) - \mu_a p_{20}(\partial m_a/\partial p_2)] \tag{5}$$

and

$$K_{1n} = \mu_a n_0(\partial m_a/\partial n)/[p_{40}(\partial m_g/\partial p_4) - \mu_a p_{20}(\partial m_a/\partial p_2)] \tag{6}$$

2.2. **Compressibility equation of compressor.** According to the compressor efficiency η_C, the compressor pressure ratio π_C of the ideal adiabatic process and the temperature difference, the air temperature at the outlet of the compressor can be obtained as follows

$$T_2 = T_1 \left\{ 1 + 1/\eta_C \left[\pi_C^{(\gamma_a - 1)/\gamma_a} - 1 \right] \right\} \tag{7}$$

where γ_a is the adiabatic index of air, η_C the adiabatic efficiency of the compressor, T_1 the air temperature at the compressor inlet and T_2 the air temperature at the compressor outlet [9].

Perform a small deviation linearization on Equation (7) to obtain the following equation:

$$\overline{T_2} = K_{2p_2} \overline{p_2} \tag{8}$$

where K_{2p_2}, the coefficient of action of $\overline{p_2}$ for $\overline{T_2}$, can be calculated by

$$K_{2p_2} = \left[(\gamma_a - 1)/\gamma_a \right] \pi_C^{(\gamma_a - 1)/\gamma_a} \Big/ \left[\eta_C + \pi_C^{(\gamma_a - 1)/\gamma_a} - 1 \right] \tag{9}$$

2.3. **The heat balance equation of the combustor.** Neglecting the heat input to the fuel temperature, the amount of heat fed into the combustor is equal to the amount of heat emitted from the combustion chamber, which is:

$$m_a c_{pa} T_3 + m_f \eta_B Q_{LHV} = m_g c_{pg} T_4 \tag{10}$$

where c_{pa} and c_{pg} are the constant air pressure specific heat capacity and the constant pressure gas heat capacity respectively, T_3 and T_4 are the combustor inlet air temperature and the combustor outlet air temperature which is equal to the turbine inlet temperature respectively, η_B stands for the combustion efficiency, m_f and Q_{LHV} stand for fuel quantity and the low calorific value of fuel respectively.

Perform a small deviation linearization on Equation (10) to obtain the following equation:

$$\overline{m_f} = K_{3n} \overline{n} + K_{3T_4} \overline{T_4} - K_{3T_3} \overline{T_3} \tag{11}$$

where the coefficient of action of $\overline{n}$ for $\overline{m_f}$ can be calculated by

$$K_{3n} = \frac{n_0}{m_{a0}} \frac{\partial m_a}{\partial n} \tag{12}$$

Similarly, the coefficient of action of $\overline{T_4}$ for $\overline{m_f}$ can be obtained by

$$K_{3T_4} = \mu_a T_{40} / \left[\mu_a T_{40} - T_{30} \left(c_{pa}/c_{pg} \right) \right] \tag{13}$$

and the coefficient of action of $\overline{T_3}$ for $\overline{m_f}$ can be calculated by

$$K_{3T_3} = T_{30} K_{2p_2} / \left[\mu_a T_{40} \left(c_{pg}/c_{pa} \right) - T_{30} \right] \tag{14}$$

2.4. **Equation of the MGT rotor.** The torque diagram of the MGT rotor is shown in Figure 2. The single axis MGT drives the rotor shaft of the generator.

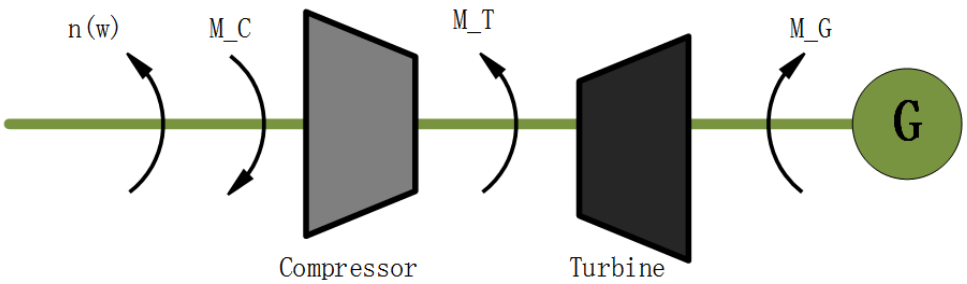

FIGURE 2. Torque diagram of MGT rotor

In the following moment balance equation, the sum of the torque consumed by the compressor and the load of generator should be equal to the torque from the turbine

$$M_T = M_C + M_G \tag{15}$$

where M_T, M_C and M_G are the torque from the turbine, the torque consumed by the compressor and the load moment respectively.

The output torque of the turbine and the compressor consumption torque are presented as follows:

$$M_T = \frac{30}{\pi}\frac{m_g c_{pg} T_4 \eta_T}{n}\left\{1 - 1\Big/\pi_T^{[(\gamma_g-1)/\gamma_g]}\right\} \tag{16}$$

$$M_C = \frac{30}{\pi}\frac{1}{n}\frac{m_a c_{pa} T_1}{\eta_C}\left\{\pi_C^{[(\gamma_a-1)/\gamma_a]} - 1\right\} \tag{17}$$

After a small deviation linearization, we have the gas turbine rotor motion equilibrium equation as follows:

$$(T_n s + 1)\,\overline{n} = K_{4T_4}\overline{T_4} + K_{4p_2}\overline{p_2} - \overline{M_G} M_{G0}\big/K_{4n} \tag{18}$$

where $T_n = [n_0\,(\pi/30)\,J]/K_{4n}$, J is the moment of inertia, $K_{4n} = M_{T0} - M_{C0} + \frac{n_0 M_{C0}}{m_{a0}}\frac{\partial m_a}{\partial n}$ and $K_{4T_4} = \frac{M_{T0}}{2K_{4n}}$.

2.5. **Equation of turbine expansion.** Based on the meaning of the efficiency η_T of the turbine's ideal adiabatic process and the definition of the expansion ratio π_T, the turbine outlet gas temperature T_5 can be expressed by

$$T_5 = T_4\left\langle 1 - \eta_T\left\{1 - 1\Big/\pi_T^{[(\gamma_g-1)/\gamma_g]}\right\}\right\rangle \tag{19}$$

where turbine expansion ratio $\pi_T = p_4/p_5$.

After a small deviation linearization, the turbine expansion equation can be formulated as follows:

$$\overline{T_4} - \overline{T_5} = K_{5p_2}\overline{p_2} \tag{20}$$

where K_{5p_2} can be calculated by

$$K_{5p_2} = \eta_T\,[(\gamma_g - 1)/\gamma_g]\Big/\left\{\eta_T + (1-\eta_T)\,\pi_T^{[(\gamma_g-1)/\gamma_g]}\right\} \tag{21}$$

2.6. **Equation of reheater dynamic.** There is a heat exchange process between the average temperature of gas, wall and air. Three heat exchange equations can be written as follows:

$$\begin{cases} m_a c_{pa}(T_3 - T_2) = \alpha_a A_a\left(T_w - \dfrac{T_2 + T_3}{2}\right) \\ m_g c_{pg}(T_5 - T_6) = \alpha_g A_g\left(\dfrac{T_5 + T_6}{2} - T_w\right) \\ m_w c_{pw}\dfrac{dT_w}{dt} = \alpha_g A_g\left(\dfrac{T_5 + T_6}{2} - T_w\right) - \alpha_a A_a\left(T_w - \dfrac{T_2 + T_3}{2}\right) \end{cases} \tag{22}$$

where T_6 is the temperature at the outlet, T_2 the reheater inlet air temperature, T_3 the outlet temperature and T_w the average temperature of the metal wall.

Combining the differential equations established in the simple cycle process, the reheater model is available as follows:

$$\begin{cases} T_3 = \dfrac{\alpha_a A_a}{m_a c_{pa} + \frac{1}{2}\alpha_a A_a} T_w + \dfrac{m_a c_{pa} - \frac{1}{2}\alpha_a A_a}{m_a c_{pa} + \frac{1}{2}\alpha_a A_a} T_2 \\ T_6 = \dfrac{\alpha_g A_g}{m_g c_{pg} + \frac{1}{2}\alpha_g A_g} T_w + \dfrac{m_g c_{pg} - \frac{1}{2}\alpha_g A_g}{m_g c_{pg} + \frac{1}{2}\alpha_g A_g} T_5 \end{cases} \tag{23}$$

where α_a is the heat transfer coefficient of air and metal wall, α_g the heat transfer coefficient of gas and metal wall, A_g the gas side heat transfer area and A_a represents the air side heat exchange area. c_{pw} stands for the constant pressure specific heat capacity of metal wall and T_w represents the average temperature of the metal wall.

2.7. **MGT system model.** Combining the above differential equations of the thermodynamic cycle with the regenerator model, the following MGT system model can be obtained by eliminating some intermediate variables

$$\begin{cases} K_{1n}\overline{n} + K_{1T_4}\overline{T_5} + \left(K_{1T_4}K_{5p_2} - 1\right)\overline{p_2} = 0 \\ K_{3n}\overline{n} + \left(K_{3T_4} - K_{3T_3}G_{12}\right)\overline{T_5} + \left(K_{3T_4}K_{5p_2} - K_{3T_3}K_{2p_2}G_{11}\right)\overline{p_2} = \overline{m_f} \\ \left(T_n s + 1\right)\overline{n} - K_{4T_4}\overline{T_5} - \left(K_{4T_4}K_{5p_2} + K_{4p_2}\right)\overline{p_2} = -\frac{M_{G0}}{K_{4n}}\overline{M_G} \end{cases} \tag{24}$$

The model of a WR100 MGT operating at the rated operating point can be obtained and described by following transfer function

$$\begin{bmatrix} \overline{n}(s) \\ \overline{T_5}(s) \end{bmatrix} = \begin{bmatrix} \dfrac{3.5327s + 0.3842}{37.2916s^2 + 1.3732s + 1} & -\dfrac{3.4325s + 0.1654}{37.2916s^2 + 1.3732s + 1} \\ \dfrac{11.9858s^2 - 6.4553s - 0.8438}{37.2916s^2 + 1.3732s + 1} & \dfrac{7.4066s + 0.6755}{37.2916s^2 + 1.3732s + 1} \end{bmatrix} \begin{bmatrix} \overline{m_f}(s) \\ \overline{M_G}(s) \end{bmatrix} \tag{25}$$

3. **Generalized Predictive Controller Design.** Generalized predictive controller becomes popular by utilizing predictive model, receding horizon optimization and feedback correction.

3.1. **Predictive model.** The predictive model can predict the future output of the system based on the system's historical data. The following CARIMA model (26) is used as a predictive model for GPC [10]

$$A\left(z^{-1}\right)y(k) = B\left(z^{-1}\right)u(k-1) + C\left(z^{-1}\right)\xi(k)/\Delta \tag{26}$$

where $A(z^{-1})$, $B(z^{-1})$ and $C(z^{-1})$ are the n-order, m-order and n-order polynomials of z^{-1} respectively; $y(k)$, $u(k-1)$ and $\xi(k)$ denote output, input and white noise sequences with mean zero respectively; $C(z^{-1}) = 1$.

3.2. **Receding horizon optimization.** In order to enhance the robustness of the control system, the response of the future time of the system based on the current control variable and output variable is considered. The following objective function is utilized to solve designed GPC controller

$$\begin{aligned} J = &\sum_{j=1}^{n} [y(k+j) - w(k+j)]^T Q [y(k+j) - w(k+j)] \\ &+ \sum_{j=1}^{m} [\Delta u(k+j-1)]^T \lambda [\Delta u(k+j-1)] \end{aligned} \tag{27}$$

where n is the maximum prediction horizon, and in general, it should be greater than the order of $B(z^{-1})$. m stands for the control length ($m \leq n$); Q and λ are positive semi-definite weighting matrixes respectively.

The goal of generalized predictive control is to find $\Delta u(k)$, $\Delta u(k+1)$, ..., $\Delta u(k+m-1)$ by minimizing the objective function (27). Combining the left and right sides of Equation (26) and multiplying them by $E_j\left(z^{-1}\right)\Delta$, then substituting following Dioaphantine Equation (28) into it

$$I = E_j\left(z^{-1}\right)A\left(z^{-1}\right)\Delta + z^{-j}F_j\left(z^{-1}\right) \tag{28}$$

where $E_j\left(z^{-1}\right) = e_{j0} + e_{j1}z^{-1} + \cdots + e_{j,j-1}z^{-j+1}$, $e_{j0} = 0$, $F_j\left(z^{-1}\right) = f_{j0} + f_{j1}z^{-1} + \cdots + f_{jn}z^{n}$.

The prediction equations for the j steps ahead can be obtained as follows:

$$y(k+j) = E_j\left(z^{-1}\right) B\left(z^{-1}\right) \Delta u(k+j-1) + F_j\left(z^{-1}\right) y(k) \tag{29}$$

Let $G_j\left(z^{-1}\right) = E_j\left(z^{-1}\right) B\left(z^{-1}\right) = g_{j0} + g_{j1}z^{-1} + \cdots + e_{jj}z^{-j} + \cdots$, and the optimal output prediction can be formulated by

$$\hat{Y} = G\Delta U + f \tag{30}$$

where

$$\hat{Y} = \left[\hat{y}(k+1), \hat{y}(k+2), \ldots, \hat{y}(k+n)\right]^T \tag{31}$$

$$\Delta U = [\Delta u(k), \Delta u(k+1), \ldots, \Delta u(k+n-1)]^T \tag{32}$$

$$f = [f(k+1), f(k+2), \ldots, f(k+n)]^T \tag{33}$$

and

$$G = \begin{pmatrix} g_0 & \cdots & 0 \\ \vdots & \ddots & \vdots \\ g_{n-1} & \cdots & g_0 \end{pmatrix} \tag{34}$$

The desired trajectory is $W = [w(k+1), w(k+2), \ldots, w(k+n)]^T$, and consequently, the objective function (20) can be reformulated by

$$J = (Y-W)^T Q(Y-W) + \Delta U^T \lambda \Delta U \tag{35}$$

After replacing Y with its optimal predictor $\hat{Y}$, let $\frac{\partial J}{\partial \Delta U} = 0$, and we have

$$\Delta U = \left(G^T G + \lambda I\right)^{-1} G^T (W - f) \tag{36}$$

In practice, the first line of ΔU is extracted and applied to the MGT systems.

3.3. **Feedback correction.** At each instant, the actual output is measured and compared with the forecast. Even if there are nonlinearity, time-varying, model mismatch and interference in the actual MGT system, the predicted output can be corrected in time. Not only can the requirements on the basic model be reduced, but also the control performance can be improved [11].

4. **Application of Generalized Predictive Control Algorithm in MGT System.** Control systems play a key role in ensuring MGT power generation systems to operate safely and efficiently. The controlled variables of the MGT power generation system are fuel quantity m_f and the torque consumed by the load moment M_G respectively, correspondingly, the manipulated variables are the rotor speed n and the turbine outlet gas temperature T_5 respectively.

In order to test the performance of the proposed GPC algorithm of the MGT power generation system shown in Figure 3. The following tests are conducted to verify tracking ability and disturbance rejection performance. GPC is compared with the traditional PID controller whose parameters are tuned by Matlab software.

4.1. **Setpoint tracking test.** The responses of the rotor speed and its set-point are shown in Figure 4. The set-point of rotor speed n_r increases from 61000 rmp to 67100 rmp at 200 s, and then decreases to 61000 rmp at 600 s. It can be seen from Figure 4 that the rotor speed can track its set-point from $t = 200$ s to $t = 600$ s. Similarly, the responses of the turbine outlet gas temperature T_5 and its set-point are shown in Figure 4. The set-point of turbine outlet gas temperature T_5 increases from 927.56 K to 1020.35 K at 1400 s, and then decreases to 927.56 K at 1400 s. It can be seen from Figure 4 that the controlled variable T_5 can track its set-point from $t = 1400$ s to $t = 1800$ s. The variations of the manipulated variables are shown in Figure 5. Compared with the traditional PID controller, the generalized predictive controller achieves a shorter settling time.

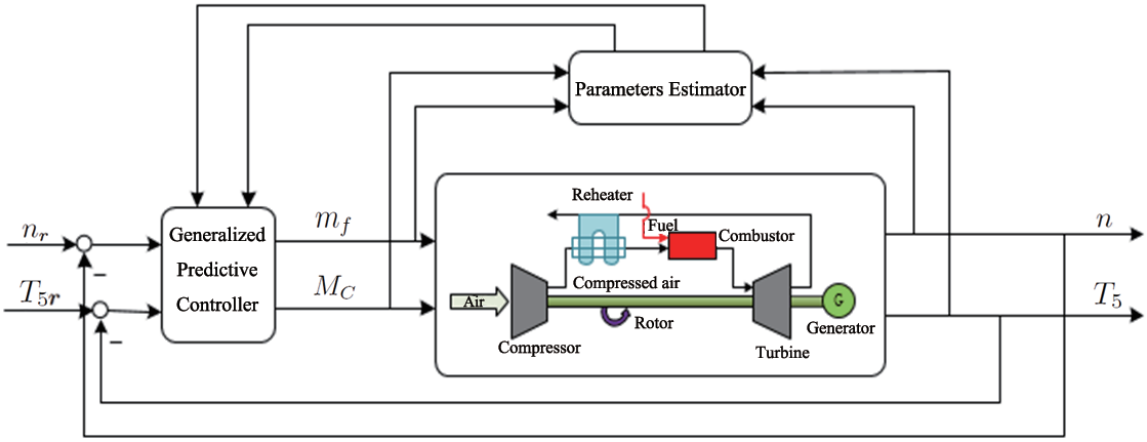

FIGURE 3. MGT power generation system input and output schematic

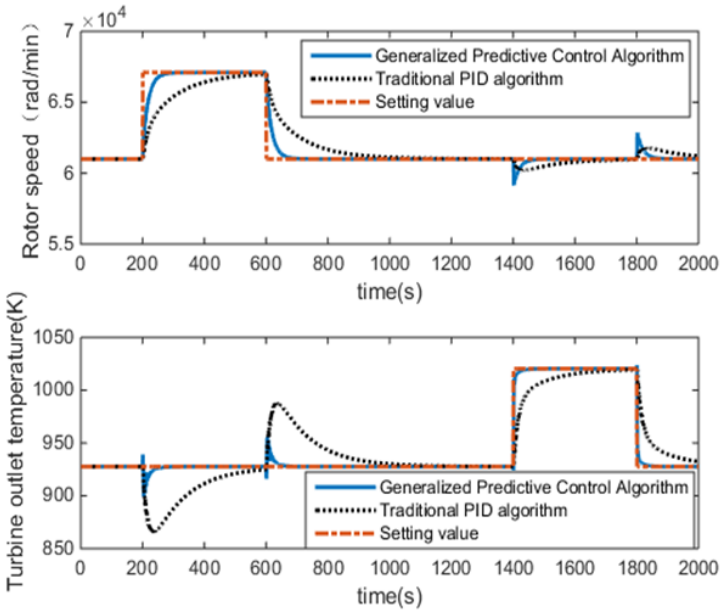

FIGURE 4. Controlled response curve

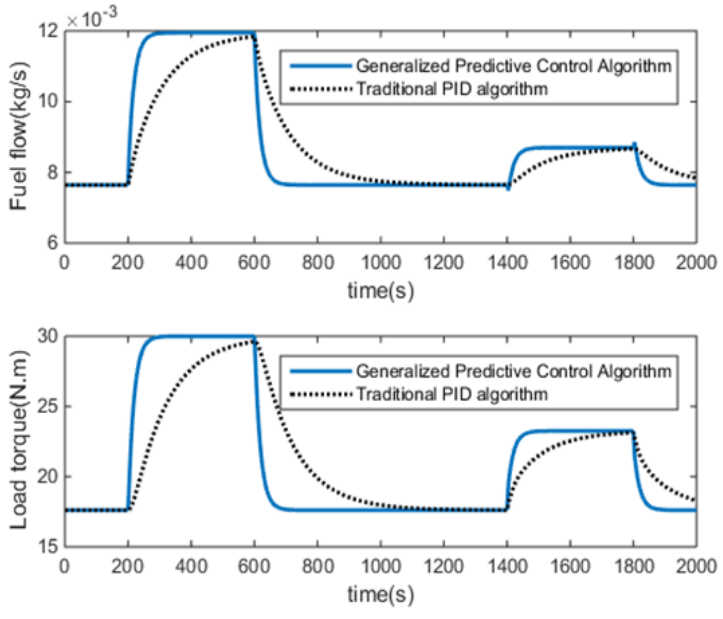

FIGURE 5. Control volume response curve

4.2. **Disturbance rejection test.** It is shown in Figure 6 that the fuel quantity m_f increases from 7.643 g/s to 8.025 g/s from 200 s to 250 s, then decreases from 8.025 g/s to 7.643 g/s between 650 s and 700 s, and the load moment M_G increases from 17.61 N·m to 18.49 N·m, and then decreases from 18.49 N·m to 17.61 N·m between 1650 s and 1700 s. The variations of the manipulated variables are shown in Figure 7. It can be seen from Figure 7 that the rotor speed n and the turbine outlet gas temperature T_5 begin to deviate from the stable operating conditions under the disturbance. Then, the controller quickly adjusts n and T_5 return to stable operating conditions.

Traditional PID controller generates control signals using linear combinations of deviations, integrals of deviations and differentials of deviations. The working process of MGT is a dynamic process. The differential term in the traditional PID controller is very sensitive to noise, which leads to the poor robustness of the traditional PID control. Compared with the traditional PID controller, the GPC has smaller overshoot and settling time.

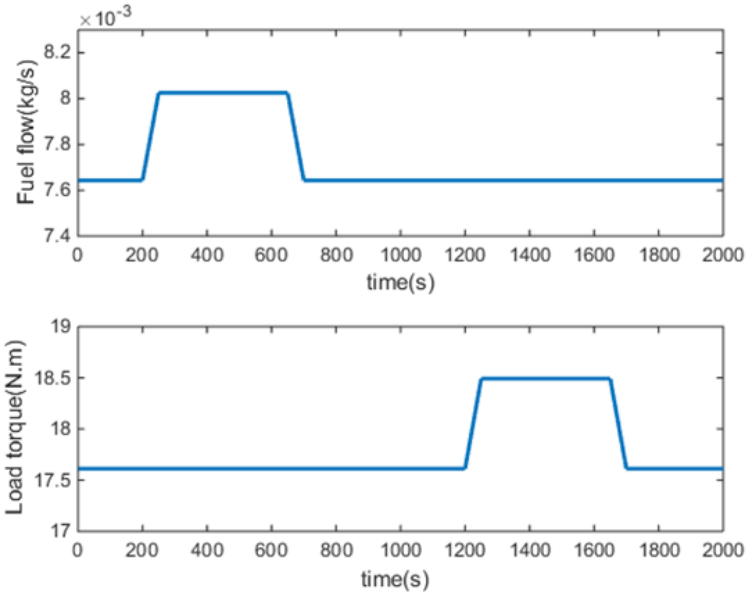

FIGURE 6. Control volume change curve

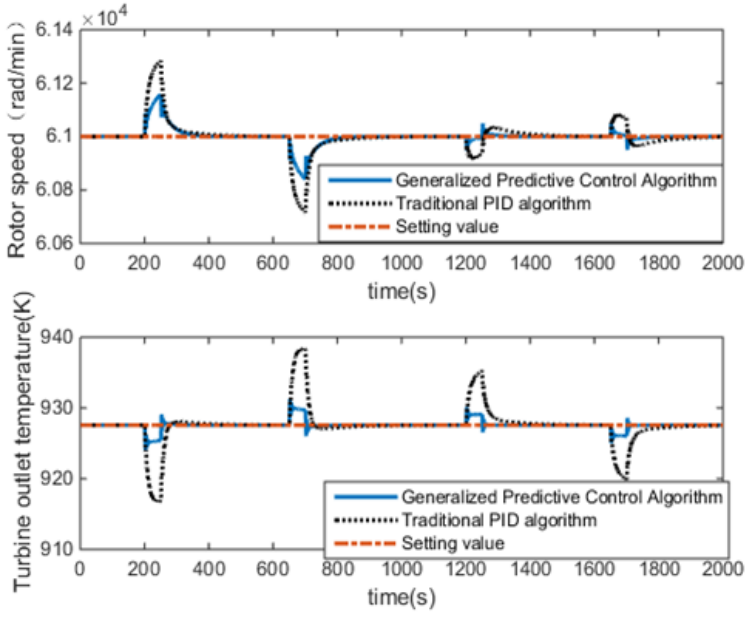

FIGURE 7. Controlled response curve

5. **Conclusion.** In this paper, the model of MGT with a reheater is established at first. Then the control quality under both traditional PID controller and GPC controller are applied to MGT system for comparison. The simulation results show that the designed GPC controller can control the MGT system more effectively and exhibit better control performance than PID controller. The further researches are as follows. On the one hand, the physical model established in this paper is a linearized model at the rated operating point, and it cannot accurately reflect the nonlinear characteristics of the original system. Therefore, the establishment of an accurate nonlinear system model is the main direction of the next study. On the other hand, although GPC shows better control performance when compared with traditional PID simulations, it is still necessary to seek other advanced control algorithms to improve control performance for MGT power systems operating over a wide range.

Acknowledgements. This work was supported by the Natural Science Foundation of China (61603136) and the Fundamental Research Funds for the Central Universities (2016ZZD03). These are gratefully acknowledged.

REFERENCES

[1] A. S. Lebedev, A. Y. Pavlov, F. Richter and A. A. Adamchuk, Experience gained from operation of the GTE-160 gas turbine installation and prospects for its modernization, *Thermal Engineering*, vol.60, no.2, pp.89-91, 2013.

[2] M. Rahman and A. Malmquist, Modeling and simulation of an externally fired micro gas turbine for standalone poly-generation application, *Journal of Engineering for Gas Turbines and Power*, vol.138, no.11, 2016.

[3] X. J. Wu, Q. Huang and X. J. Zhu, Power decoupling control of a solid oxide fuel cell and micro gas turbine hybrid power system, *Journal of Power Sources*, vol.196, no.3, pp.1295-1302, 2011.

[4] L. C. Saikia and S. K. Sahu, Automatic generation control of a combined cycle gas turbine plant with classical controllers using firefly algorithm, *International Journal of Electrical Power and Energy Systems*, vol.53, no.1, pp.27-33, 2013.

[5] M. Khashei, M. Bijari and G. A. R. Ardali, Improvement of auto-regressive integrated moving average models using fuzzy logic and artificial neural networks (ANNs), *Neurocomputing*, vol.72, no.4, pp.956-967, 2009.

[6] D. T. Peng, C. Q. Zhang and Q. K. Peng, Design of improved generalized predictive controller in the critical thermal process of 600MW subcritical unit, *Chinese Control Conference*, pp.4277-4282, 2016.

[7] M. Samavati, Polygeneration system based on low temperature solid oxide fuel cell/micro gas turbine hybrid system, *Energiteknik*, 2012.

[8] K. Peng, D. Fan, F. Yang, Q. Fu and Y. Li, Active generalized predictive control of turbine tip clearance for aero-engines, *Chinese Journal of Aeronautics*, vol.26, no.5, pp.1147-1155, 2013.

[9] D. Barsi, A. Perrone, Y. Qu, L. Ratto, G. Ricci and V. Sergeev, Compressor and turbine multidisciplinary design for highly efficient micro-gas turbine, *Journal of Thermal Science*, vol.27, no.3, pp.259-269, 2018.

[10] C. H. Lu and C. C. Tsai, Generalized predictive control using recurrent fuzzy neural networks for industrial processes, *Journal of Process Control*, vol.17, no.1, pp.83-92, 2007.

[11] M. Gulan, M. Salaj and B. Rohal'-Ilkiv, Real-time implementation of an adaptive feedback and feedforward generalized predictive controller, *International Conference on Process Control*, pp.383-388, 2013.